



## UvA-DARE (Digital Academic Repository)

### Cardiac microvascular dysfunction

*Insights from COVID-19, myocardial infarction, and anthracycline-induced cardiotoxicity*

Jiang, Z.

#### Publication date

2026

[Link to publication](#)

#### Citation for published version (APA):

Jiang, Z. (2026). *Cardiac microvascular dysfunction: Insights from COVID-19, myocardial infarction, and anthracycline-induced cardiotoxicity*. [Thesis, fully internal, Universiteit van Amsterdam].

#### General rights

It is not permitted to download or to forward/distribute the text or part of it without the consent of the author(s) and/or copyright holder(s), other than for strictly personal, individual use, unless the work is under an open content license (like Creative Commons).

#### Disclaimer/Complaints regulations

If you believe that digital publication of certain material infringes any of your rights or (privacy) interests, please let the Library know, stating your reasons. In case of a legitimate complaint, the Library will make the material inaccessible and/or remove it from the website. Please Ask the Library: <https://uba.uva.nl/en/contact>, or a letter to: Library of the University of Amsterdam, Secretariat, P.O. Box 19185, 1000 GD Amsterdam, The Netherlands. You will be contacted as soon as possible.

# Chapter 7

## **Exposure of endothelial cells to Doxorubicin inhibits Extracellular matrix production by dermal fibroblasts in a paracrine manner**

Zhu Jiang *MEng*, Giulia Sorrentino *BSc*, Madalena Lopes Natário Pinto Gomes *MEng*, Amber Swan-Taylor, Suat Simsek *MD PhD*, Joris J.T.H. Roelofs *MD PhD*, Hans W.M. Niessen *MD PhD*, Paul A.J. Krijnen *PhD*.

**Running title:** Endothelial–Fibroblast Crosstalk in Doxorubicin Toxicity

**Under Revision in :**

*Toxicological Sciences.*

1

2

3

4

5

6

7

8

9

10

## Abstract

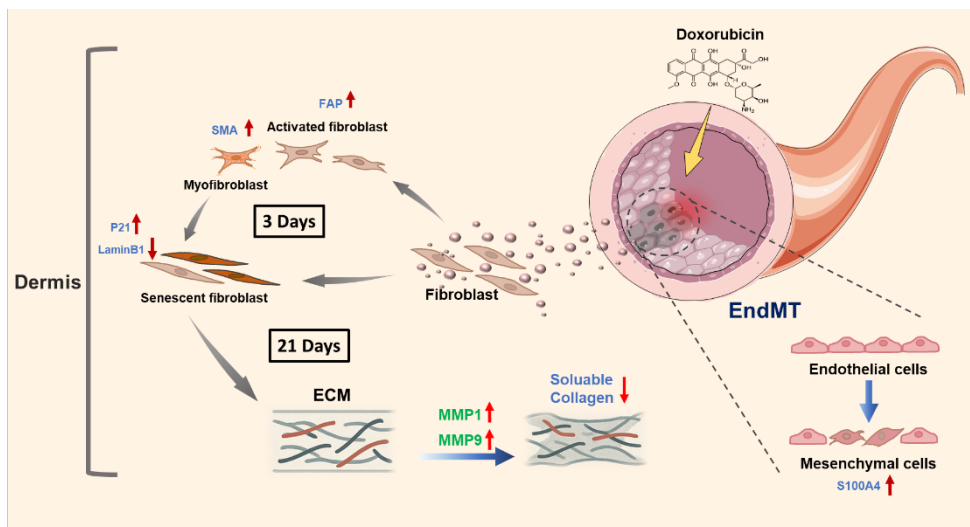
Doxorubicin (Dox) is a potent chemotherapeutic with known vascular toxicity and connective-tissue damage. Endothelial cells (EC) and fibroblasts crosstalk is essential for vascular homeostasis and extracellular matrix (ECM) remodeling. This study aimed to explore whether Dox induces endothelial-to-mesenchymal transition (EndMT) and the paracrine effects of Dox-exposed EC on fibroblasts activation, senescence, and ECM synthesis.

Human umbilical vein endothelial cells (HUVECs) were treated with Dox, and conditioned medium (CM) from EC was applied to human dermal fibroblasts for short- and long-term culture. Dox induced EndMT in ECs. Fibroblasts exposed to CM from Dox-treated EC exhibited early activation with increased fibroblast activation protein (FAP) and  $\alpha$ -smooth muscle actin ( $\alpha$ -SMA) at day 3, followed by a progressive senescent phenotype marked by elevated p21 and reduced Lamin B1 at day 21. ECM formation was impaired, with reduced collagen and increased transcriptional expression of matrix-degrading enzymes (MMP1 and MMP9). Cytokines profiling of the CM revealed decreased interleukin-1 $\beta$  (IL-1 $\beta$ ), C-C motif ligand 2 (CCL2) and C-X-C motif ligand 10 (CXCL10), and elevated interleukin-6 (IL-6) levels.

These findings demonstrate that exposure of EC to Dox induced endothelial dysfunction and elicited pathological paracrine signaling, driving fibroblast activation, myofibroblast transition, senescence, and ECM disruption. This mechanism may underlie Dox-related skin aging and delayed wound healing and emphasized the importance of endothelial dysfunction in chemotherapy-associated connective tissue damage and impaired repair.

**Keywords:** Doxorubicin; Endothelial dysfunction; Fibroblast; Paracrine signaling; Extracellular matrix remodeling.

## Graphical Abstract



## Highlights:

- Doxorubicin (Dox) triggers endothelial-to-mesenchymal transition (EndMT)
- Dox-induced endothelial paracrine signaling causes fibroblast activation and senescence
- Dox-induced endothelial paracrine signaling impairs collagen production and elevates metalloproteinase expression
- Endothelial–fibroblast crosstalk mediates chemotherapy-induced tissue injury

## 1. Introduction

Doxorubicin (Dox) is a widely used anthracycline chemotherapeutic agent, effective against various malignancies<sup>[1]</sup>. However, its clinical application is significantly limited by well-documented dose-dependent cardiotoxicity<sup>[2]</sup>. Increasing attention has also been directed toward its systemic toxicity, affecting multiple organs and the vasculature<sup>[3,4][5]</sup>. In the skin, Dox has been associated with impaired wound healing<sup>[6]</sup>, skin necrosis<sup>[7]</sup>, and reduced regenerative capacity<sup>[8]</sup>.

The skin is a highly vascularized organ, where dynamic interactions between vascular cells are essential for maintaining tissue integrity and regulating injury

response. Endothelial cells (ECs), which form the inner layer of blood vessels, play important roles in vascular barrier function, inflammatory regulation, and paracrine signaling<sup>[9]</sup>. During intravenous chemotherapy, ECs are directly exposed to Dox and are particularly susceptible to damage. Fibroblasts, key mediators of extracellular matrix (ECM) synthesis, wound healing, angiogenesis, and fibrosis, are also critical for tissue repair and homeostasis<sup>[10]</sup>. Dysregulated fibroblast activity during chemotherapy can exacerbate disease progression. In Dox-induced cardiotoxicity models, activated fibroblasts are primary contributors to ECM accumulation and myocardial fibrosis<sup>[11]</sup>. In vitro studies have demonstrated that Dox can trigger pro-inflammatory responses and induce cellular senescence in fibroblasts<sup>[12]</sup>.

One key mechanism of endothelium dysfunction is the endothelial-to-mesenchymal transition (EndMT), in which ECs lose endothelial markers and acquire mesenchymal properties. EndMT has been linked to pro-fibrotic activity and development of fibrosis in various pathological progression, including cardiac fibrosis<sup>[13]</sup> and pulmonary fibrosis in mice<sup>[14]</sup>, as well as post myocardial infarction remodeling in human<sup>[15]</sup>. Additionally, under pathological conditions, ECs released a complex secretome of proteins and biomolecules which is crucial for endothelial behavior regulation, intercellular communication and shaping tissue microenvironment<sup>[16]</sup>. For instance, ECs undergoing EndMT in obese adipose tissue released paracrine or endocrine signals that modulated neighboring vascular and stromal cells<sup>[17]</sup>.

Moreover, dysfunctional endothelial cells can adopt a senescence-associated secretory phenotype, characterized by the release of cytokines and growth factors that promote inflammation, thrombosis, and vascular dysfunction<sup>[18-20]</sup>. In chronic kidney disease, an altered endothelial secretome has been implicated in tubulointerstitial fibrosis<sup>[21]</sup>.

While vascular injury is increasingly recognized as a driver of Dox-induced fibrosis, its role in modulating fibroblast behavior in the skin remains poorly understood. In particular, the impact of Dox on skin vasculature and dermal ECM homeostasis has yet to be fully elucidated.

In this study, we investigated the effects of Dox on endothelial-fibroblast crosstalk using a human cell model. EndMT was assessed in HUVECs following Dox treatment, and the endothelial secretome was collected. The Dox-induced EC secretome was applied to human dermal fibroblast to evaluate alterations in

activation markers, senescence indicators and ECM remodeling over short-term (3 days) and long-term (21 days) periods.

## 2. Materials and Methods

### 2.1 Materials and cells

Chemicals and reagents used in this study are listed in **Table S1**. Human Umbilical Vein Endothelial Cells (HUVECs) were purchased from ScienCell (#8000, Carlsbad, CA, USA) and cultured in Endothelial Cell Medium with endothelial cell growth supplement, antibiotic solution, and fetal bovine serum (FBS) (ECM; ScienCell). Healthy skin fibroblasts were obtained from the Burn Research Lab, Alliance of Dutch Burn Care, Beverwijk, The Netherlands. Fibroblasts were isolated from seven donors (five female, one male, one unknown sex; mean age  $50 \pm 6$  years). The use of the coded, post-operative residual tissue materials was approved by patients through the informed opt-out-plus protocol of the Red Cross Hospital (<https://www.coreon.org/wp-content/uploads/2023/06/Code-of-Conduct-for-Health-Research-2022.pdf>). Fibroblast isolation was performed as previously described [22]. The fibroblasts were cultured in Dulbecco's Modified Eagle Medium (DMEM, 41966029, ThermoFisher, USA), supplemented with 10% FBS (F7524, Sigma-Aldrich, St. Louis, MO, USA), 1% penicillin-streptomycin (15140-122, Thermo Scientific, USA) and 1% GlutaMAX (35050-038, Thermo Scientific, USA), referred to as complete DMEM. Doxorubicin hydrochloride (#DM1515, Sigma-Aldrich, St. Louis, MO, USA) was dissolved in Dimethylsulfoxide (DMSO) to prepare a 15 mM stock solution and stored at  $-80^{\circ}\text{C}$ .

### 2.2 Cell culture

The experimental set up was shown in **Figure 1**. The HUVECs and fibroblast were cultured at  $37^{\circ}\text{C}$  in a humidified 5%  $\text{CO}_2$  environment. Cells used in all experiments were passage 2-4.

HUVECs were seeded in 6-well or 24-well plates. For immunofluorescent analysis, cells were cultured on glass coverslips in 24-well plates. When the cells reached approximately 90% confluence, they were exposed to ECM containing Dox at a final concentration of  $10 \mu\text{M}$  for 1 hour or  $1 \mu\text{M}$  for 24 hours. These Dox concentrations were chosen to model acute and prolonged exposure respectively, based on the pharmacokinetic studies indicating that peak plasma Dox concentration

in patients can exceed 10  $\mu\text{M}$  before gradually declining<sup>[23]</sup>. As Dox was dissolved in DMSO, a control medium containing an equivalent concentration of DMSO was used. Following Dox exposure, the medium was replaced with fresh ECM, and the cells were maintained for 7 days, with medium changes every two days.

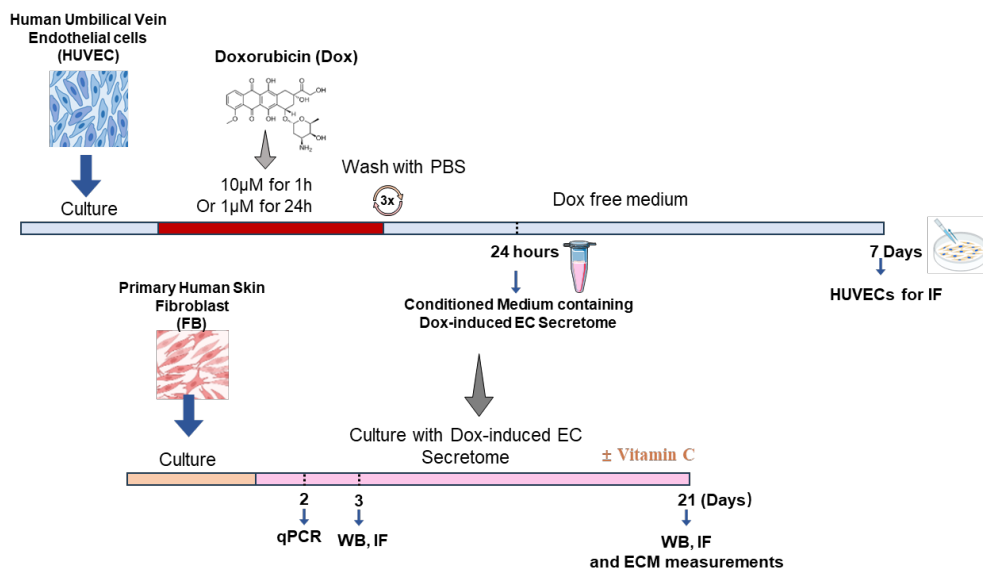


**Figure 1. Experimental design.**

Shown is a graphical outline of the experimental design of this study. For evaluating Dox-induced EndMT, HUVECs were exposed to Dox, (10  $\mu\text{M}$  for 1 h; or 1  $\mu\text{M}$  for 24 h), followed by 7-day recovery in Dox-free medium to assess EndMT using immunofluorescent microscopy (IF). To assess the paracrine effects of Dox-exposed EC on dermal fibroblasts, conditioned medium (CM) was collected from HUVEC cultures, 24 hours after exposure to Dox or DMSO. This CM was then applied to primary human dermal fibroblasts up to 21 days of culture, with or without supplemented magnesium ascorbyl phosphate (VitC). The effects of CM on fibroblast activation and senescence were assessed at 3 and 21 days (WB or/and IF); on collagen synthesis (WB, collagen assay, eosin staining) was evaluated at 21 days; and on MMP1 and MMP9 gene expression (qPCR) at 2 days.

To obtain the secretome of endothelial cells, after Dox or DMSO exposure HUVECs were cultured in fresh complete DMEM for 24 hours, after which the conditioned medium was collected. Fibroblasts were cultured in fresh complete DMEM in 24-well plates. For immunofluorescent experiments the cells were cultured in 24-well plates on glass coverslips. After the fibroblasts reached approximately 90% confluence, they were cultured in conditioned medium, which was refreshed every two days, for a culture duration ranging from 2 days to 21 days. Given the essential role of vitamin C (ascorbic acid) as a cofactor in ECM synthesis, magnesium ascorbyl phosphate, a stable vitamin C derivative that is enzymatically converted to

ascorbic acid in cells, was added to the conditioned medium for the 21-day cultures at a final concentration of 10 µg/mL.

### 2.3 Western Blot

The cells were scraped from wells and lysed with sample buffer containing 4% (v/v) SDS, 18% (v/v) Glycerol and 0.2M Tris-HCL (pH 6.8). Protein concentration of prepared samples was determined using Pierce BCA Protein Assay kit (23225, Thermo Scientific, USA) and absorbance at 562 nm was measured with CLARIO star Plus microplate reader. Equal amounts of protein were calculated and prepared for loading by mixing samples with laemmli buffer (4% v/v SDS, 18% v/v Glycerol, 2% v/v β-mercaptoethanol, 0.002% w/v Bromophenol blue dissolved in 0.2M (pH 6.8) Tris-HCL), followed by heating for 5 min at 95 °C. For the supernatant samples' preparation, equal volumes of the supernatant were mixed with laemmli buffer in a 1:1 ratio and heated at 95 °C for 5 min.

Samples were separated using NuPAGE Bis-Tris Mini Protein Gels (4–12%, 1.0–1.5 mm, NP0322BOX, Thermo Scientific, USA) at 80V for 20 min, followed by 120 V for 45 min. Proteins were transferred from gel onto a PVDF membrane at 120V for 1 hour. After extensive washing with TBST, membranes were blocked with 5% (w/v) skim milk in TBST for 1 hour at RT.

Membranes were incubated overnight at 4 °C with primary antibodies: mouse-anti-α-SMA (Dako; M0851, 1:1000), rabbit-anti-FAP (NOVUS; NBP2-66844, 1:1000), rabbit-anti-Collagen I (Abnova; PAB10190, 1:1000 dilution), or rabbit-anti-S100A4 (abcam; ab197896, 1:1000). Following three washes with TBST (TBS with 0.1%(v/v) tween 20), the membranes were incubated with secondary antibodies: rabbit-anti-mouse IgG-HRP (Dako; P0260, 1:2500 dilution) for α-SMA or goat-anti-rabbit IgG-HRP (Dako; P0448, 1:2500 dilution) for FAP, Collagen I and S100A4, for 1 hour at RT. Detection was performed using Pierce™ ECL Western Blotting Substrate (32106, Thermo Scientific, USA).

For proteins with similar molecule weights, membranes were stripped using stripping buffer (2% (v/v) SDS, 0.7% (v/v) β-mercaptoethanol, and 60 mM Tris-HCL, pH 6.7). After extensive washing with TBST, the membranes were re-blocked with a solution of 5% (w/v) skim milk in TBST for 1 hour at RT and incubated overnight at 4 °C with primary antibodies: rabbit-anti-p21 (Cell Signaling, CS2947, 1:1000 dilution), rabbit-anti-Lamin B1 (abcam; ab16048, 1:1000 dilution), or

mouse-anti- $\beta$ -actin (Sigma; A1578, 1:50000 dilution.  $\beta$ -actin served as the internal reference. After washing three times with TBST, membranes were incubated with secondary antibodies: rabbit-anti-mouse IgG-HRP (Dako; P0260, 1:2500 dilution) for  $\beta$ -actin or goat-anti-rabbit IgG-HRP (Dako; P0448, 1:2500 dilution) for p21 and LaminB1, for 1 hour at RT. Visualization steps were performed as described above. Western blot bands were quantified using Image J. Target protein intensities ( $\alpha$ -SMA:44kDa; FAP: both 80 and 88 kDa; S100A4: 12 kDa; Lamin B1: 68 kDa; p21: 21 kDa; Collagen I: 139 kDa) were normalized to housekeeping protein  $\beta$ -actin (44 kDa) within the same lane. Fold changes were calculated relative to corresponding control samples.

## 2.4 Immunofluorescent staining

For immunofluorescent staining, cells were fixed after treatment with 4% paraformaldehyde for 10 minutes at RT and subsequently permeabilized using 0.1% (v/v) Triton X-100 in PBS for 10 min. After extensive PBS washes, cells were blocked with a solution of 1% BSA and 0.1% NaN<sub>3</sub> in PBS and then incubated with primary antibodies: mouse-anti- $\alpha$ -SMA (Dako; M0851, 1:1000) or rabbit-anti-FAP (NOVUS; NBP2-66844, 1:1000) for 2 hours at RT. After washing three times with PBS, cells were incubated with secondary antibodies: goat-anti-rabbit IgG(H+L) A633 (Thermo Fisher Scientific; A21070, 1:500 dilution) for FAP or goat-anti-mouse IgG(H+L) A488 (Thermo Fisher Scientific; A11029, 1:500 dilution) for  $\alpha$ -SMA, for 1 hour at RT. Hoechst (1:1000) was used for nuclear counterstaining. After staining, cells were mounted with Prolong Gold antifade reagent (P36934; Thermo Fisher Scientific) onto glass slides. Cells that were stained without primary antibody and without any antibody served as negative controls. A Leica DMi8 inverted microscope equipped with a Leica TCS SP8 X DLS camera was used to image the slides at 600 $\times$  magnification.

## 2.5 Collagen detection and Morphology quantification

Eosin staining was used to visualize and quantify ECM produced by fibroblasts in culture. After 21 days of culture, fibroblasts were washed three times with PBS, stained with 200  $\mu$ L of 1% eosin solution for 2 minutes, and rinsed five times with PBS. Images of each well were acquired using a digital camera, and staining intensity was quantified using QuPath v0.6.0. Insoluble and soluble collagen levels were measured using Sircol<sup>TM</sup> Collagen Kits (S1000, S2000, Biocolor Ltd, UK) following the manufacturer's instructions.

For morphological assessment, brightfield images of fibroblasts in culture were captured at 200× magnification using an inverted light microscope equipped with a digital camera. Cellular morphology was quantified by determining the elongation factor, calculated as the ratio of maximum cell length to maximum cell width. Per image the average of 10-20 cells was used.

## 2.6 RNA isolation, cDNA synthesis and quantitative real-time PCR (qRT-PCR)

Fibroblasts were harvested after 2-day culture of conditioned medium. RNA was extracted using TRI Reagent (T9424, Sigma-Aldrich) following the acid guanidinium thiocyanate-phenol-chloroform extraction method [24]. cDNA synthesis was performed using M-MLV reverse transcriptase (28025013, Thermo Fisher Scientific) according to the manufacturer's protocol. qRT-PCR was conducted with cDNA using primers listed in **Table 1**. The primers were synthesized using Eurogentec (Maastricht, The Netherlands). Reactions were performed with sensiFAST SYBR master mix (BIO-98005, Biorun reagents, London, UK) on Roche LightCycler 480 platform. *YWHAZ* and *GPI* served as the internal reference genes. Reaction without template DNA served as a negative control. Cycling conditions as follows: 95°C for 2 min, followed by 50 three-step cycles of 95°C for 5 s, 65°C for 10 s, and 72°C for 10 s.

qRT-PCR results were analyzed using LC480 Conversion, LinRegPCR and LightCycler 480.

**Table 1. Primers used in this study**

Gene	Protein	Primers	Sequence (5'-3')
<i>MMP1</i>	MMP1	Forward	TCGGGGAGAAGTGATGTTCT
<i>MMP9</i>	MMP9	Forward	CGGACCAAGGATACAGTTTGT
<i>YWHAZ</i>	YWHAZ	Forward	CATCTTGAGGGTCGTCTCA
<i>GPI</i>	GPI	Forward	GACGGCGAAGGAGTGTTTC

List of genes, corresponding proteins, and primer sequences used for qPCR. Forward and reverse indicate primer orientation, sequences are shown in the 5'-3' direction.

Abbreviations: MMP1: Matrix metalloproteinase-1; MMP9: Matrix metalloproteinase-9; YWHAZ: Tyrosine 3-monooxygenase/tryptophan 5-Monooxygenase activation protein zeta ; GPI: Glucose-6-phosphate isomerase.

## 2.7 Cytokine measurement in Dox-induced EC secretome

The cytokine composition of the conditioned media (CM) from Dox- and DMSO-treated ECs was measured using LEGENDplex™ Human Essential Immune Response Panel (13plex, 740930, BioLegend), following the manufacturer's instructions.

## 2.8 Statistics

GraphPad Prism (version 9, San Diego, CA, USA) was used for the design and generation of graphs. Statistical analyses were conducted using GraphPad Prism, SPSS (version 26.0, Armonk, NY, USA), and Excel (2016, Microsoft, USA). Each experiment was replicated a minimum of three times. t-tests were applied to compare two groups. One-way analysis of variance (ANOVA) was applied to compare three or more groups. Data were presented using mean  $\pm$  standard deviation (SD), p value below 0.05 was considered statistically significant.

## 3. Results

### 3.1 Dox treatment induced endothelial-to-Mesenchymal Transition (EndMT)

To investigate whether Dox treatment induces EndMT, HUVECs were treated with 10  $\mu$ M Dox for 1 hour or 1  $\mu$ M Dox for 24 hours followed by culture in Endothelial Cell Medium for 7 days. Immunofluorescence analysis showed a significant upregulation of fibroblast biomarker S100A4 in HUVECs treated with both Dox concentrations compared with cells treated with DMSO-containing medium or untreated cells (control) (**Figure 2A**). S100A4 expression was respectively 6.5  $\pm$  5.0-fold and 6.2  $\pm$  3.1-fold higher in 10  $\mu$ M and 1  $\mu$ M Dox-treated cells compared with untreated cells (both  $p < 0.05$ ) (**Figure 2B**). CD31 expression (marker of endothelial cells) showed no significant changes compared to DMSO-treated or untreated cells (**Figure 2C**). Exposure to the vehicle DMSO had no significant effects on S100A4 expression compared with untreated cells (data not shown).

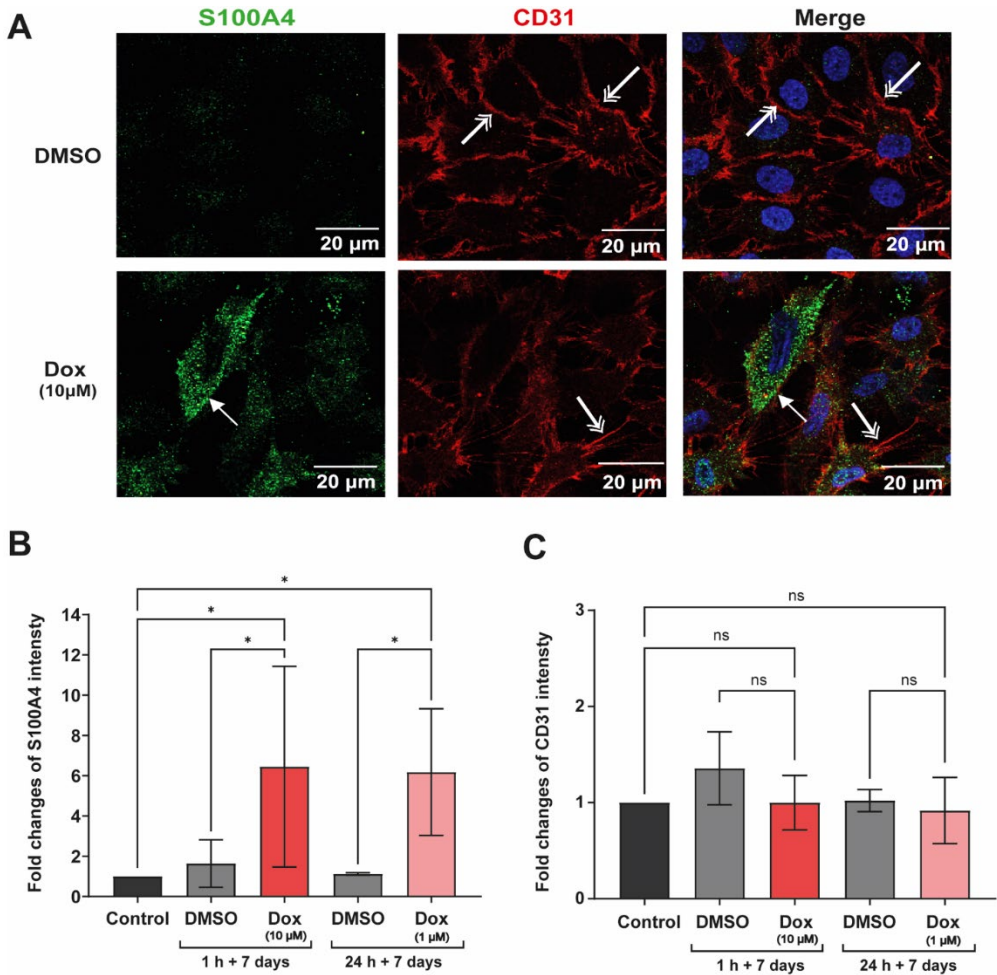


**Figure 2** Dox treatment-induced effects on endothelial-to-Mesenchymal Transition (EndMT).

(A) Representative immunofluorescence images of S100A4 and CD31 staining in HUVECs show increased S100A4 expression 7 days after Dox treatment (10 μM, 1h), indicating induced EndMT. White arrows indicate CD31-positive cell membranes (red), while double-head white arrows indicate cytoplasmic S100A4 positivity (green). Nuclei were counterstained with Hoechst in blue, as shown in the merged images.

(B - C) Quantification of S100A4 and CD31 expression in HUVECs treated with Dox (10 μM for 1h or 1 μM for 24h), assessed by quantifying the relative fluorescence intensity from immunofluorescence images. 15 images per condition were analyzed across three individual experiments (n = 3), using identical imaging settings. Data are represented as Mean ± SD. \*p<0.05, ns indicates not significant.

### 3.2 Paracrine effects of Dox-exposed EC on fibroblast activity and myofibroblast transition

To investigate the effect of the secretome from Dox-treated endothelial cells on fibroblast activation and myofibroblast transition, fibroblasts from 7 donors were cultured in conditioned medium (CM) from HUVECs treated with 10  $\mu$ M Dox for 1 hour ( $\text{CM}^{\text{Dox}10}$ ) or 1  $\mu$ M Dox for 24 hours ( $\text{CM}^{\text{Dox}1}$ ) or equivalent DMSO concentrations ( $\text{CM}^{\text{DMSO}10}$  or  $\text{CM}^{\text{DMSO}1}$ ), for 3 days (short-term) or 21 days (long-term) (**Figure 1**). For the 21-day cultures, the CM was supplemented with 10  $\mu$ g/mL VitC.

Fibroblast activation and myofibroblast transition were assessed via quantification of the expression of fibroblast activation marker FAP, myofibroblast marker  $\alpha$ -SMA, and fibroblast marker S100A4. Immunofluorescence staining revealed cytoplasmic localization of FAP (red) and filamentous  $\alpha$ -SMA (green) structures characteristic of respectively fibroblast activation and myofibroblast differentiation (**Figure 3A**).

WB analysis confirmed the presence of FAP (distinct bands at  $\sim$ 80-88 kDa, representing different forms of FAP<sup>[25]</sup>),  $\alpha$ -SMA (42 kDa) and S100A4 (12 kDa), both after 3 and 21 days (**Figure 3B**). After 3 days,  $\text{CM}^{\text{Dox}10}$ -treated fibroblasts had significantly increased FAP ( $1.3 \pm 0.3$ -fold,  $p < 0.05$ ) and  $\alpha$ -SMA ( $1.4 \pm 0.3$ -fold,  $p < 0.05$ ) protein levels, while S100A4 protein levels did not differ significantly compared to  $\text{CM}^{\text{DMSO}10}$ -treated cells (**Figure 3C**). Similarly,  $\text{CM}^{\text{Dox}1}$ -treated fibroblasts showed significantly higher FAP ( $1.4 \pm 0.4$ -fold,  $p < 0.05$ ) and  $\alpha$ -SMA ( $1.4 \pm 0.5$ -fold,  $p < 0.05$ ) levels, with similar S100A4 levels compared to  $\text{CM}^{\text{DMSO}1}$ -treated cells (**Figure 3D**).

After 21 days, sustained significant upregulation of FAP ( $1.5 \pm 0.3$ -fold,  $p < 0.05$ ) was observed in  $\text{CM}^{\text{Dox}10}$ -treated fibroblasts, in the absence of VitC, but not when VitC was present (**Figure 3C**). While in  $\text{CM}^{\text{Dox}1}$ -treated cells no significant changes in FAP or  $\alpha$ -SMA were observed compared to  $\text{CM}^{\text{DMSO}1}$ -treated cells, either with or without VitC (**Figure 3D**).

These results show that Dox-induced EC secretome promotes dermal fibroblast activation and myofibroblast transition, especially in response to higher Dox concentrations.

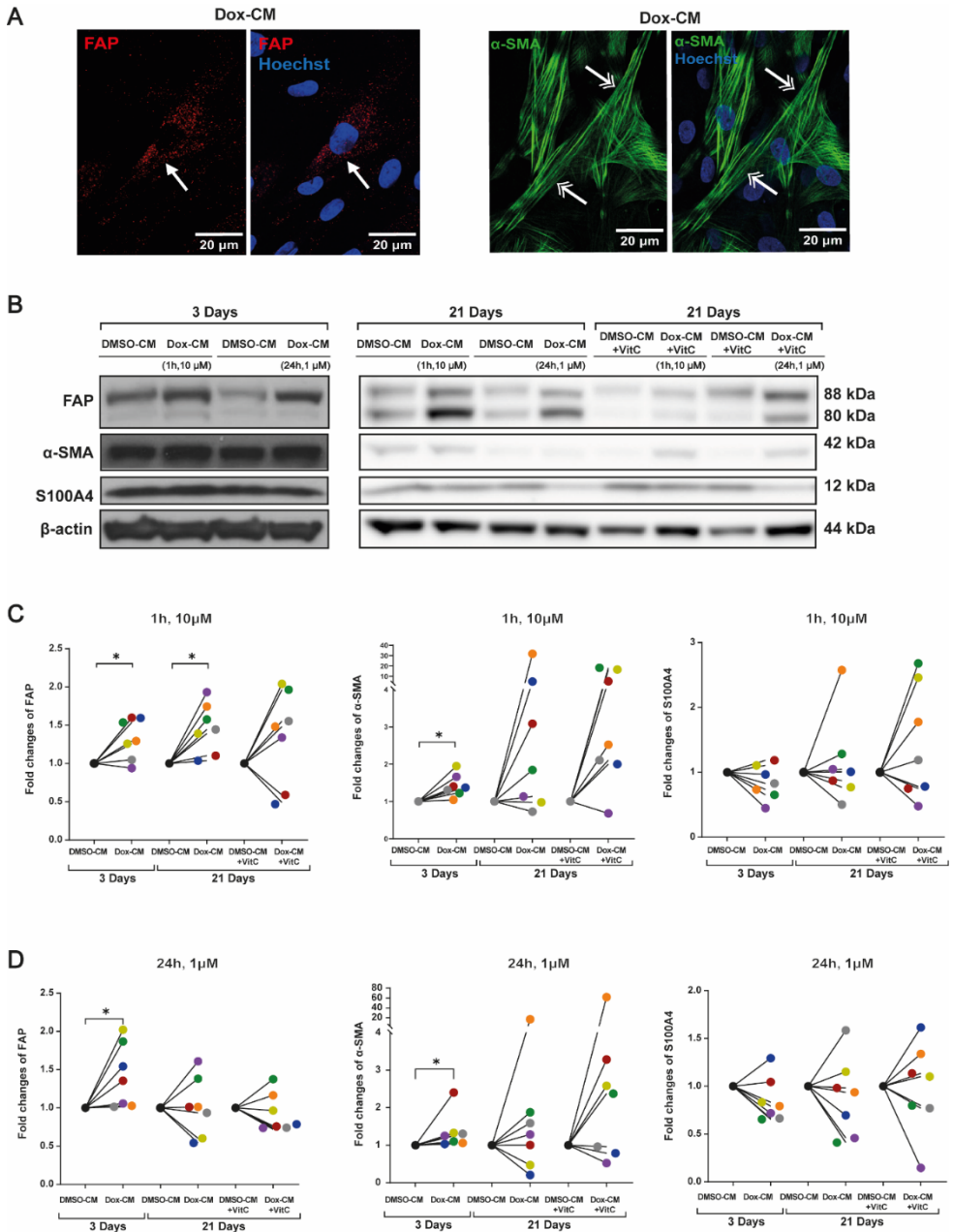


**Figure 3** Paracrine effects of Dox-exposed EC on fibroblast activity and myofibroblast transition

(A) Representative immunofluorescence images showing FAP (red) and  $\alpha$ -SMA (green) in human dermal fibroblasts treated with conditioned medium (CM) harvested from HUVECs that were exposed to Dox ( $10 \mu\text{M}$ , 1h) for 3 days. White arrows indicate cytoplasmic FAP; Double-head white arrows indicate filamentous  $\alpha$ -SMA. Nuclei were counterstained with Hoechst in blue, as shown in the merged images. (B) Representative Western blot (WB)

images showing bands for FAP,  $\alpha$ -SMA, S100A4, and  $\beta$ -actin in human dermal fibroblasts treated with CM harvested from HUVECs exposed to Dox (Dox-CM) or equivalent doses of DMSO (DMSO-CM) for 3 days or 21 days (with or without magnesium ascorbyl phosphate (VitC)). (C-D) Quantification of WB results for FAP,  $\alpha$ -SMA and S100A4 expression, relative to  $\beta$ -actin, in human dermal fibroblasts from seven individual donors ( $n = 7$ ), treated with CM harvested from HUVECs exposed to Dox (Dox-CM) or equivalent doses of DMSO (DMSO-CM), with/without VitC, for 3 or 21 days. The results for CM of HUVECs exposed to 10 $\mu$ M Dox (or DMSO) for 1h are shown in (C) and for CM of HUVECs exposed to 1 $\mu$ M Dox (or DMSO) for 24h are shown in (D). Data is shown normalized to fibroblasts treated with DMSO-CM. \* $p < 0.05$ .

### 3.3 Paracrine effects of Dox-exposed EC on fibroblast senescence

To evaluate fibroblast senescence in response to Dox-induced EC secretome, fibroblasts from 7 donors were cultured for either 3 days or 21 days in CM. Cells were then assessed for morphological changes and analyzed by WB for protein levels of the senescence marker p21 and the negative senescence marker Lamin B1 [26].

Both CM<sup>Dox10</sup>- and CM<sup>Dox1</sup> treatments induced a significant elongation of fibroblasts compared to CM<sup>DMSO10</sup>- and CM<sup>DMSO1</sup> treatments both with and without VitC (**Figure 4A**, left). The cellular elongation factors in response to CM<sup>Dox10</sup> ( $17.7 \pm 2.3$  (-VitC) and  $18.7 \pm 2.2$  (+VitC)) and CM<sup>Dox1</sup> ( $17.8 \pm 2.0$  (-VitC) and  $21.0 \pm 3.4$  (+VitC)) more than doubled compared to CM<sup>DMSO10</sup> ( $8.5 \pm 0.9$  (-VitC) and  $8.0 \pm 0.7$  (+VitC)) and CM<sup>DMSO1</sup> ( $8.3 \pm 1.5$  (-VitC) and  $8.5 \pm 0.4$  (+VitC))( $p < 0.0001$  for all; **Figure 4A** right). VitC had no significant additional effects on cell morphology.

WB analysis showed p21 as a distinct band at 21 kDa and Lamin B1 at 68 kDa (**Figure 4B**). In CM<sup>Dox10</sup>-treated fibroblasts p21 expression significantly increased compared to CM<sup>DMSO10</sup>-treated cells at both time points, with a  $2.0 \pm 1.1$ -fold at 3 days and a further increase to  $2.5 \pm 1.0$ -fold at day 21 ( $p < 0.05$  for both) (**Figure 4C**). The presence of VitC enhanced this CM<sup>Dox10</sup>-induced increase in p21 expression to  $7.0 \pm 3.9$ -fold compared CM<sup>DMSO10</sup>-treated cells ( $p < 0.05$ ). In parallel, CM<sup>Dox10</sup> significantly decreased Lamin B1 protein levels to  $0.6 \pm 0.2$ -fold at 3 days and further reduced to  $0.4 \pm 0.1$ -fold by day 21 ( $p < 0.05$  for both) compared to CM<sup>DMSO10</sup> treatment. This decrease appeared more pronounced in the presence of VitC, with Lamin B1 expression decreasing to  $0.2 \pm 0.1$ -fold ( $p < 0.05$ ) (**Figure 4C**).

A similar trend was observed in response to CM<sup>Dox1</sup> treatment where p21 expression was significantly elevated at day 3 ( $2.4 \pm 1.0$ -fold) and at day 21 ( $2.5 \pm 1.5$ -fold) ( $p < 0.05$  for both), with further enhancement by VitC supplement ( $5.1 \pm 1.6$ -fold,  $p < 0.05$ ). Lamin B1 levels decreased to  $0.6 \pm 0.3$ -fold at day 3 and  $0.5 \pm 0.1$ -fold at day

21 ( $p < 0.05$  for both) and decreased further with VitC to  $0.2 \pm 0.1$ -fold ( $p < 0.05$ ) (Figure 4D).

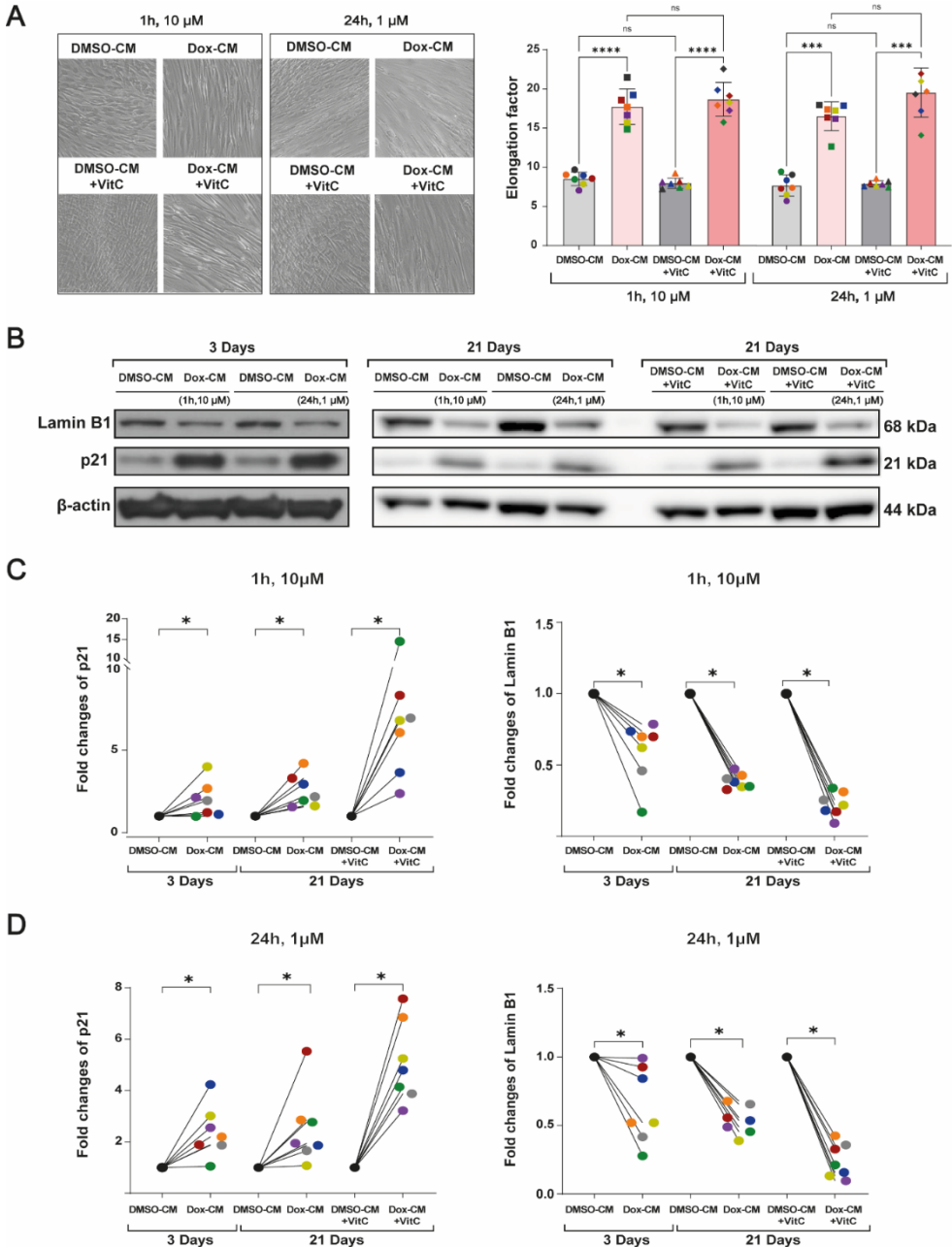


**Figure 4** Paracrine effects of Dox-exposed EC on fibroblast senescence

(A) *Left*: Representative bright field images of human dermal fibroblasts treated with conditioned medium (CM) harvested from HUVECs exposed to Dox (Dox-CM; either  $10\mu\text{M}$  for 1h or  $1\mu\text{M}$  Dox for 24h) or equivalent doses

of DMSO (DMSO-CM), for 21 days (with or without magnesium ascorbyl phosphate (VitC)). The differences in cellular morphology are visible. **Right:** Quantification of the elongation factor, calculated as the ratio of the maximum to minimum cell diameter in the treatments described under **A Left. (B)** Representative Western blot (WB) images showing bands of Lamin B1, p21, and  $\beta$ -actin in human dermal fibroblasts treated with conditioned medium (CM) from HUVECs exposed to Dox (Dox-CM; either 10 $\mu$ M for 1h or 1 $\mu$ M Dox for 24h) or equivalent doses of DMSO (DMSO-CM), for 3 days or 21 days (with or without magnesium ascorbyl phosphate (VitC)). **(C - D)** Quantification of WB results for p21 and Lamin B1 expression, relative to  $\beta$ -actin, in human dermal fibroblasts from seven individual donors ( $n = 7$ ), treated with CM harvested from HUVECs exposed to Dox (Dox-CM) or equivalent doses of DMSO (DMSO-CM), with/without VitC, for 3 or 21 days. The results for CM of HUVECs exposed to 10 $\mu$ M Dox (or DMSO) for 1h are shown in **(C)** and for CM of HUVECs exposed to 1 $\mu$ M Dox (or DMSO) for 24h are shown in **(D)**. Data is shown normalized to fibroblasts treated with DMSO-CM. \* $p < 0.05$ .

These results indicate that Dox-induced EC secretome promotes a senescent phenotype in dermal fibroblasts.

### 3.4 Paracrine effects of Dox-exposed EC on collagen production and ECM formation

To evaluate the effects of Dox-induced EC secretome on fibroblast function, fibroblasts from 7 donors were cultured in CM for 21 days with or without VitC, and subsequently analyzed for ECM formation and collagen production.

Eosin staining intensity was used to quantify ECM formation by fibroblasts (**Figure 5A left**). In the absence of VitC, eosin staining intensity after CM<sup>DMSO10</sup>-treatment was  $0.3 \pm 0.1$ , which was significantly decreased by CM<sup>Dox10</sup>-treatment ( $0.1 \pm 0.1$ ;  $p < 0.05$ ) (**Figure 5A right**). The presence of VitC significantly increased ECM deposition by CM<sup>DMSO10</sup>-treated cells to  $0.6 \pm 0.1$  ( $p < 0.01$ ), which again was significantly lowered by CM<sup>Dox10</sup>-treatment ( $0.2 \pm 0.1$ ;  $p < 0.01$ ). Similarly, CM<sup>Dox1</sup>-treatment significantly decreased eosin staining intensity to  $0.1 \pm 0.1$  (-VitC) and  $0.2 \pm 0.1$  (+VitC) compared to CM<sup>Dox10</sup>-treatment ( $0.4 \pm 0.1$  (-VitC) and  $0.5 \pm 0.1$  (+VitC);  $p < 0.05$ ) (**Figure 5A right**).

In addition, soluble and insoluble collagen in the cells and ECM were quantified using Sircol collagen assay. Soluble collagen reflects newly synthesized, non-crosslinked collagen, while insoluble collagen represents mature, crosslinked fibers integrated into the ECM. No significant difference in insoluble collagen was measured between CM<sup>Dox10</sup>-treated- and CM<sup>Dox10</sup>-treated cells, independent of VitC (**Figure 5B**). However, soluble collagen levels after CM<sup>Dox10</sup>-treatment decreased to a significant 0.2  $\pm$  0.3-fold of CM<sup>DMSO10</sup>-treated cells ( $p < 0.05$ ), only in the presence of VitC. In CM<sup>Dox1</sup>-treated cells, in the presence of VitC, insoluble collagen levels were significantly reduced to 0.6  $\pm$  0.3-fold of CM<sup>DMSO1</sup>-treated cells ( $p < 0.05$ ),

while soluble collagen levels were significantly decreased both in the absence ( $0.5 \pm 0.3$ -fold;  $p < 0.05$ ) and presence of VitC ( $0.1 \pm 0.1$ -fold;  $p < 0.0001$ ) compared to  $CM^{DMSO1}$  (**Figure 5C**).

To assess whether the observed inhibitory effects on ECM formation are related to an inhibitory effect of collagen crosslinking rather than production, the levels of collagen type 1 (collagen-1) protein were quantified via WB in the supernatants of the cultures that were collected across three time windows (day 1-7, 8-14, and 15-21) (**Figure 5D**). This time-resolved analysis accounts for the cumulative and dynamic secretion of ECM proteins, thereby enabling a more accurate assessment of temporal changes in collagen release and potential impairment in collagen crosslinking or stabilization.

Collagen-1 levels in the supernatant of  $CM^{Dox10}$ - and  $CM^{Dox1}$ -treated cells in all three-time windows were significantly lower than those in the supernatant of  $CM^{DMSO10}$ - and  $CM^{DMSO1}$ -treated cells, regardless of the presence of VitC (**Figure 5E**,  $p < 0.05$  for all). The presence of VitC significantly enhanced the levels of collagen-1 ( $2.0 \pm 1.3$ -fold or higher) in the supernatant of both  $CM^{DMSO10}$ - and  $CM^{DMSO1}$ -treated fibroblasts (**Figure 5E**;  $p < 0.05$  for all). Of note, collagen-1 levels in the supernatant after  $CM^{DMSO}$ -treatment did not differ significantly relative to fibroblasts cultured in standard DMEM (data not shown). Although VitC also significantly enhanced collagen-1 levels in the supernatant of  $CM^{Dox10}$ - and  $CM^{Dox1}$ -treated cells ( $p < 0.05$ ; apart from not significant at day 1-7 in  $CM^{Dox10}$ ), this effect was less pronounced.

These results suggest that the Dox-induced EC secretome significantly impairs collagen production and ECM formation.

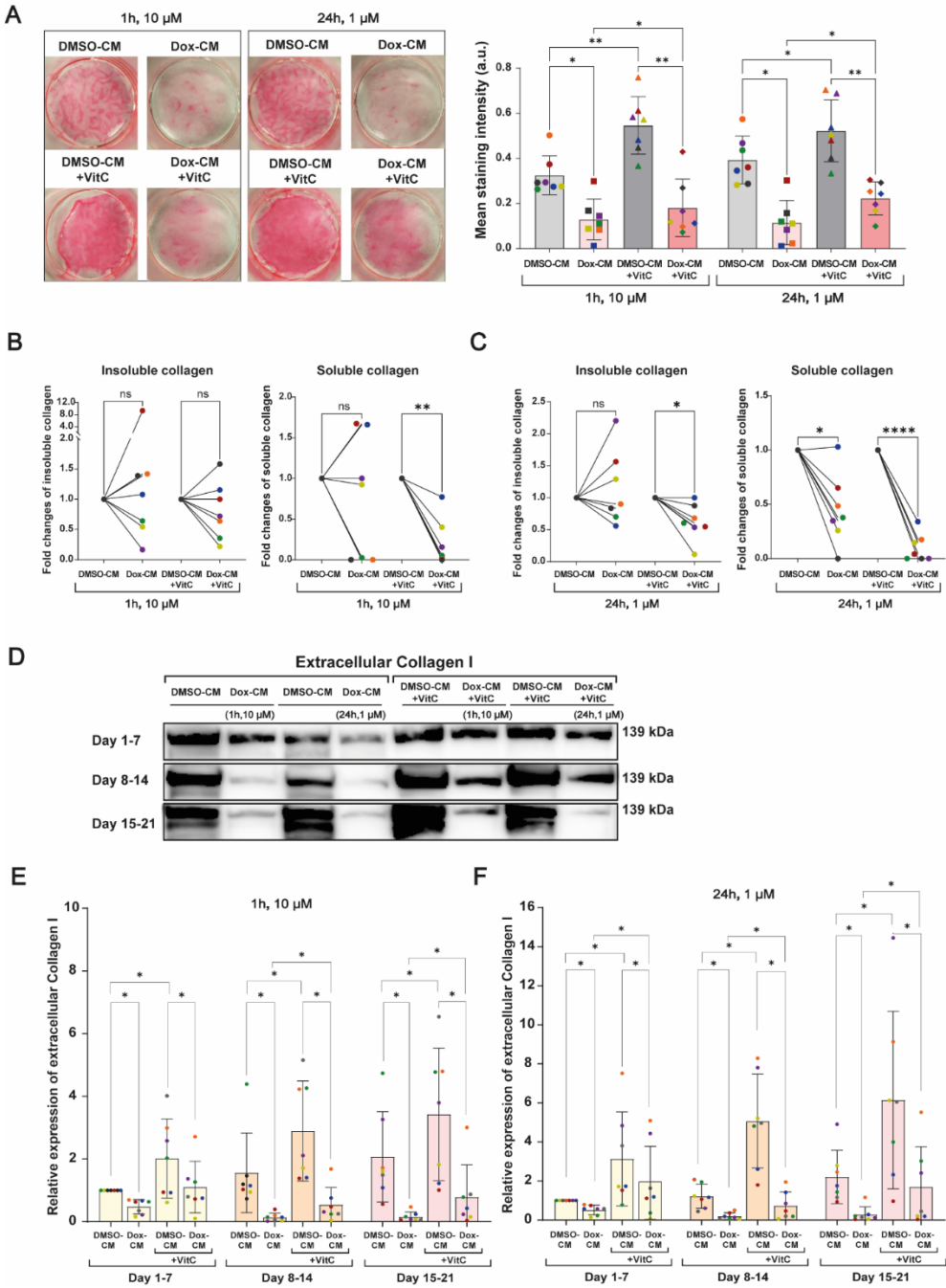


**Figure 5** Paracrine effects of Dox-exposed EC on fibroblast collagen production and ECM formation

(A) **Left:** Representative eosin staining images of human dermal fibroblasts treated with conditioned medium (CM) harvested from HUVECs exposed to Dox (Dox-CM; either 10 $\mu$ M for 1h or 1 $\mu$ M Dox for 24h) or equivalent doses of DMSO (DMSO-CM), for 21 days (with or without magnesium ascorbyl phosphate (VitC)). Formed ECM stains red. **Right:** Quantification of the eosin staining intensities in the treatments described under A Left. (B–C) Quantification of insoluble collagen and soluble collagen levels in the harvested fibroblasts + ECM after the treatment described under A left. The results for CM of HUVECs exposed to 10 $\mu$ M Dox (or DMSO) for 1h are shown in (B) and for CM of HUVECs exposed to 1 $\mu$ M Dox (or DMSO) for 24h are shown in (C). (D) Representative Western blot (WB) images showing Collagen I expression in the supernatants of human dermal fibroblasts treated as described in (A). Supernatant was collected daily and from each donor the samples from days 1-7, 8-14, and 15-21 were combined to form three groups over time. (E–F) Quantification of supernatant Collagen I levels from human dermal fibroblasts, from seven individual donors (n = 7), treated as described in (A). The results for CM of HUVECs exposed to 10 $\mu$ M Dox (or DMSO) for 1h are shown in (E) and for CM of HUVECs exposed to 1 $\mu$ M Dox (or DMSO) for 24h are shown in (F). Data is shown normalized to the supernatant of fibroblasts treated with DMSO-CM. \*p<0.05; \*\*p<0.01; \*\*\*p<0.001; \*\*\*\*p<0.0001 and ns indicates not significant.

### 3.5 Paracrine effects of Dox-exposed EC on the transcriptional levels of MMP1 and MMP9

Matrix metalloproteinases (MMPs) are ECM-degrading enzymes that can be produced by fibroblasts, and MMP1 and MMP9 have been shown to be involved in skin ageing<sup>[27]</sup>. To evaluate the effects of Dox-induced EC secretome MMP1 and MMP9 expression, fibroblasts from 7 donors were cultured in CM for 2 days, with or without VitC, and subsequently harvested for qRT-PCR analysis.

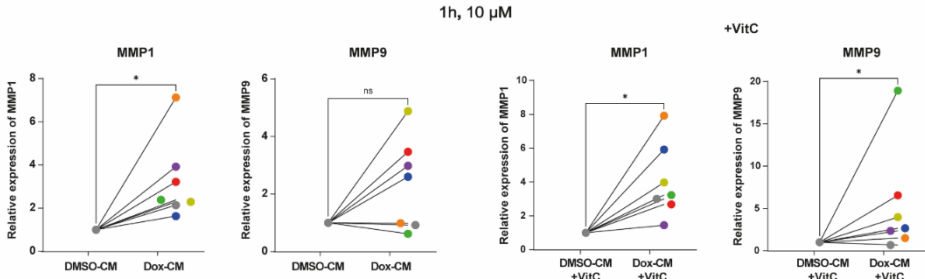
CM<sup>Dox10</sup>-treatment resulted in a significant 3.2  $\pm$  1.9-fold increase in MMP1 transcription (p<0.05), and a borderline significant 2.4  $\pm$  1.6-fold increase in MMP9 transcription (p=0.0644) compared to CM<sup>DMSO10</sup>. These effects were enhanced in the presence of VitC, where CM<sup>Dox10</sup>-treatment increased MMP1- and MMP9 transcriptional levels 4.0  $\pm$  2.2-fold and 5.2  $\pm$  6.3-fold respectively (p<0.05 for both) (**Figure 6A**). Similarly, CM<sup>Dox1</sup>-treatment significantly increased MMP1- and MMP9 transcriptional levels 4.1  $\pm$  3.8-fold and 7.6  $\pm$  5.4-fold (p < 0.05 for both) compared to CM<sup>DMSO1</sup>, while VitC supplementation amplified this response especially for MMP1, whose transcriptional levels increased 16.9  $\pm$  22.4-fold compared to CM<sup>DMSO1</sup>, while MMP9 remained at 7.6  $\pm$  5.4-fold (p<0.05 for both) (**Figure 6B**).

### 3.6 Inflammatory cytokine changes in Dox-induced EC secretome

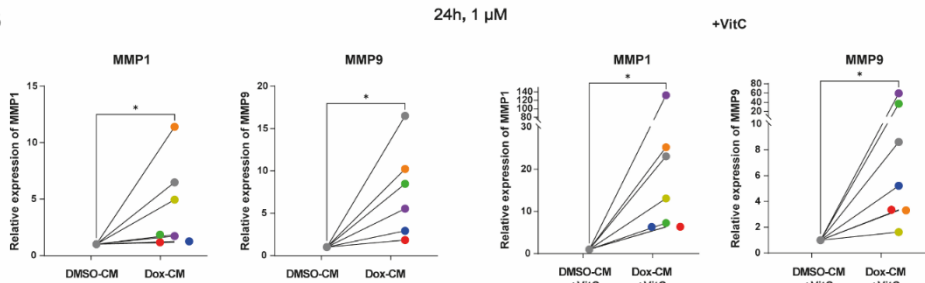
The cytokine composition of the conditioned medium (CM) from Dox-treated ECs was analyzed using a multiplex bead-based immunoassay, which simultaneously quantified IL-4, IL-2, CXCL10 (IP-10), IL-1 $\beta$ , TNF- $\alpha$ , CCL2 (MCP-1), IL-17A, xl,

IL-10, IL-6, IFN- $\gamma$ , IL-12p70, CXCL8 (IL-8) and free active TGF- $\beta$ 1. Among the 13 cytokines measured, IL-4, IL-2, TNF- $\alpha$ , IL-17A, IL-10, IFN- $\gamma$ , IL-12p70 and free active TGF- $\beta$ 1 were below the detection limit ( $< 2.0$  pg/mL).

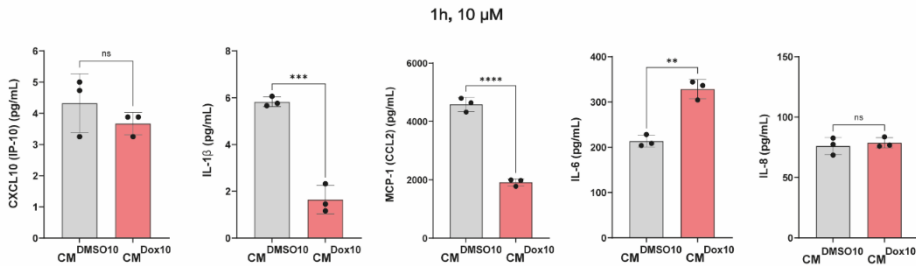
A



B



C



D

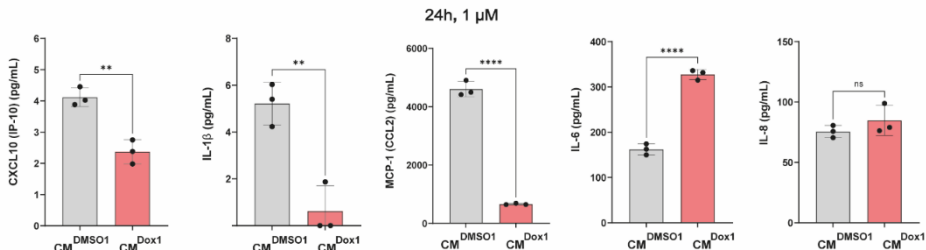


**Figure 6** Paracrine effects of Dox-exposed EC on the transcriptional levels of MMP1 and MMP9 and cytokine measurements in conditioned media

(A - B) Quantification of MMP1 and MMP9 transcriptional expression relative to YWHAZ and GPI in human dermal fibroblasts, from seven donors ( $n = 7$ ), treated with conditioned medium (CM) harvested from HUVECs exposed to Dox (Dox-CM; either (A) 10  $\mu\text{M}$  for 1h or (B) 1  $\mu\text{M}$  Dox for 24h) or equivalent doses of DMSO (DMSO-CM), for 2 days (with or without magnesium ascorbyl phosphate (VitC)). Data is shown normalized to fibroblasts treated with DMSO-CM). \* $p < 0.05$  and ns indicates not significant. (C - D) Cytokine (CXCL10 (IP-10), IL-1 $\beta$ , CCL2 (MCP-1), IL-6, CXCL8 (IL-8)) measurements in conditioned medium (CM) from HUVECs treated with 10  $\mu\text{M}$  Dox for 1 hour ( $\text{CM}^{\text{Dox}10}$ ) or 1  $\mu\text{M}$  Dox for 24 hours ( $\text{CM}^{\text{Dox}1}$ ) or equivalent DMSO concentrations ( $\text{CM}^{\text{DMSO}10}$  or  $\text{CM}^{\text{DMSO}1}$ ), data from three individual experiments ( $n = 3$ ). \*\* $p < 0.01$ ; \*\*\* $p < 0.001$ ; \*\*\*\* $p < 0.0001$  and ns indicates not significant.

Compared to  $\text{CM}^{\text{DMSO}10}$  and  $\text{CM}^{\text{DMSO}1}$  treated fibroblasts, CXCL10 (IP-10) was significantly reduced only in  $\text{CM}^{\text{Dox}1}$  ( $4.1 \pm 0.3$  vs  $2.4 \pm 0.4$  pg/mL;  $p < 0.05$ ) but remained unchanged in  $\text{CM}^{\text{Dox}10}$ . Both  $\text{CM}^{\text{Dox}10}$  and  $\text{CM}^{\text{Dox}1}$  treated fibroblasts showed significant reductions in IL-1 $\beta$  ( $5.8 \pm 0.2$  vs  $1.6 \pm 0.6$  pg/mL and  $5.2 \pm 0.9$  vs  $0.6 \pm 1.1$  pg/mL, respectively;  $p < 0.001$  for both) and CCL2 (MCP-1) ( $4585 \pm 240$  vs  $1917 \pm 122$  pg/mL and  $4603 \pm 263$  pg/mL vs  $659 \pm 27$  pg/mL, respectively;  $p < 0.0001$  for both), alongside significant increases in IL-6 ( $213 \pm 13$  vs  $328 \pm 21$  pg/mL and  $162 \pm 12$  vs  $327 \pm 11$  pg/mL, respectively;  $p < 0.0001$  for both). CXCL8 (IL-8) levels remained unchanged in both conditions (**Figure 6C and 6D**)

#### 4. Discussion

In this study, we investigated the effects of acute (1 h at 10  $\mu\text{M}$ ) and prolonged (24 h at 1  $\mu\text{M}$ ) Dox exposure on ECs, as well as the subsequent impact of their secretome on dermal fibroblast function. Our findings revealed that Dox treatment induced EndMT in HUVECs and that the Dox-induced EC secretome modulated fibroblast activation and senescence induction, ultimately resulting in suppressed collagen production and ECM synthesis during prolonged incubation.

HUVECs subjected to Dox exposure, followed by 7 days of recovery in Dox-free medium, exhibited classical EndMT characteristics, demonstrated by upregulation of fibroblast marker S100A4. The vascular implications of EndMT have been well-documented, leading to disassembly of endothelial intercellular junctions, compromised endothelial barrier integrity, impaired angiogenic capacity and fibrosis<sup>[17,28,29]</sup>. In vivo, studies have shown that Dox treatment reduced cardiac microvascular density and impaired cardiac function in mice<sup>[30]</sup>, with endothelial fate tracing confirming that EndMT-derived cells contributed to Dox-induced cardiac fibrosis<sup>[31]</sup>. The EndMT following Dox treatment observed in this study reinforced these observations, suggesting that Dox-induced EndMT may be a potential mechanism in microvascular rarefaction and tissue hypoperfusion, both of

which are critical contributors to tissue aging and impaired wound healing<sup>[32,33]</sup>. Beyond direct vascular effects, through their secretome endothelial cells exert potent paracrine effects on adjacent and even distal stromal cell populations. For instance, during physiological skin repair, endothelial-derived factors such as VEGF, EGF and PDGF promote fibroblast proliferation and ECM synthesis, facilitating re-epithelialization and collagen deposition in murine wounds<sup>[34]</sup>. However, under pathological conditions, such as EndMT in hypertrophic scars or metabolic stress in obesity, the EC secretome alters toward TGF- $\beta$ , bFGF, and endothelin-1 driving fibroblast activation/conversion and excessive matrix accumulation in dermis<sup>[35]</sup>, adipose tissue, and pressure overloaded<sup>[13]</sup> or diabetic<sup>[36]</sup> hearts. In our study, the endothelial cells exposed to Dox showed markedly elevated IL-6 secretion, but reduced IL-1 $\beta$ , CCL2 (MCP-1) and CXCL10 levels, indicating a shift in cytokine profile in their secretome. Although IL-6 upregulation is consistent with findings in Dox-treated human coronary artery endothelial cells, the study also reported modest elevated levels of IL-1 $\beta$ , IL-8 and CCL2 expression<sup>[37]</sup>, suggesting that Dox-induced cytokine responses may vary depending on endothelial cell type, exposure duration, or concentration. The elevated IL-6 levels may, in part, explain some of our observed effects on endothelial cells and fibroblasts. For instance, inhibition of autophagy in human microvascular endothelial cells induced EndMT, that could be prevented with an IL-6-neutralizing antibody, indicating that the EndMT was IL-6-dependent<sup>[38]</sup>. In addition, IL-6 has been shown to induce profibrotic activation in fibroblasts, including myofibroblast transition<sup>[39,40]</sup>, as well as senescence<sup>[41]</sup>. IL-6 may thus be an important factor in the early fibroblast activation, myofibroblast transition and senescence we observed in fibroblasts exposed to Dox-induced EC secretome. Notably, IL-1 $\beta$  and CCL2 mediate early monocyte/macrophage recruitment<sup>[42]</sup> to clear debris and guide fibroblast-mediated matrix remodeling<sup>[43]</sup> during normal tissue repair. The inhibitory effect of Dox on their production by EC observed in this study may impair critical early phases of wound healing. Moreover, in aging populations, prolonged elevated IL-6 expression has been implicated in the extended inflammatory phase of wound repair, contributing to delayed wound healing<sup>[44]</sup>, suggesting that a changed secreted cytokine profile in EC may contribute to the delayed wound healing observed in individuals undergoing chemotherapy<sup>[45]</sup>.

CM from Dox-treated ECs profoundly affected human dermal fibroblasts behavior. Fibroblasts exposed to Dox-induced EC secretome for three days showed enhanced expression of FAP, indicating increased activation of fibroblasts. Activated

fibroblasts (FAP+) contribute to pro-fibrotic activation and tissue remodeling and have been implicated in infarct tissue remodeling in myocardial infarction patients<sup>[15]</sup> and fibrotic tissue formation during skin wound repair in mice<sup>[46]</sup>. Concurrently, the expression of  $\alpha$ -SMA, a key marker of myofibroblasts, was significantly upregulated, indicating a phenotypic transition towards a contractile, fibrosis-driving state. This myofibroblast phenotype is essential for ECM remodeling and wound contraction<sup>[47]</sup>. A similar pro-fibrotic activation was shown to underlie Dox-induced cardiac fibrosis via PI3K/Akt-and Smad- dependent upregulation of  $\alpha$ -SMA, TGF- $\beta$ , and collagen<sup>[48-50]</sup>. Notably, free active TGF- $\beta$ 1 was undetectable in our CM.

The early activation of fibroblast likely represented an acute reactive fibrotic response to paracrine stress signals from dysfunctional ECs. However, prolonged exposure to Dox-induced EC secretome did not show an elevated ECM formation. Instead, fibroblasts displayed signs of senescence, including upregulation of p21 and downregulation of Lamin B1, both indicative of impaired proliferative capacity and altered secretory profiles that may further disrupt tissue repair.

Vitamin C, a well-known enhancer of collagen synthesis and ECM stabilization through the promotion of collagen molecule hydroxylation, crosslinking, and collagen expression, was supplemented in long-term culture to promote ECM formation<sup>[51]</sup>. While VitC indeed supported collagen production in fibroblasts cultured with normal EC secretome (DMSO-induced EC secretome), fibroblasts exposed to the Dox-induced EC secretome showed significantly suppressed collagen deposition despite VitC supplementation. Quantification analysis confirmed reduction in both intracellular and secreted collagen synthesis, accompanied by impaired ECM deposition visualized by eosin staining, which reflected a cumulative impact of Dox-induced endothelial dysfunctional secretome on connective tissue formation. Morphological elongation of Dox-induced EC secretome-exposed fibroblasts coincided with disrupted ECM production and increased senescence markers. Similar phenotypic changes have been observed in fibroblasts from aged skin and fibrotic tissues, where fibroblasts lose their matrix production capacity and adopt a senescence-associated secretory phenotype<sup>[52,53]</sup>.

Furthermore, qPCR analysis revealed a transcriptional upregulation of matrix metalloproteinases MMP1 and MMP9 in fibroblast treated with the Dox-induced EC secretome. Both enzymes are responsible for ECM degradation and are

commonly associated with aged human skin<sup>[54]</sup>. Elevated MMP1, which primarily targeted interstitial collagens (type I, II, and III), has been linked to collagen breakdown and skin aging in UV-exposed human skin<sup>[55]</sup>. While MMP9 degrades denatured collagens and basement membrane proteins, particularly type IV and V collagen, involved in vascular morphogenesis and angiogenesis<sup>[56,57]</sup>. Although MMP1 and MMP9 are essential for wound healing<sup>[58]</sup>, their overactivity can exacerbate collagen degradation, weaken tissue tensile strength, and contribute to the abnormal tissue remodeling, commonly observed in aging and fibrotic tissue pathology<sup>[59]</sup>. The transcriptional upregulation of both MMP1 and MMP9 observed in this study may disrupt the dermal ECM and contribute to the vascular basement membrane disruption, potentially exacerbating vascular dysfunction in Dox-treated patients.

Clinically, the mode of Dox administration has been adjusted to mitigate cardiotoxicity, with continuous intravenous infusion commonly used instead of rapid bolus injection to reduce peak plasma concentration, which have been linked to cellular damage and morphological changes in the cardiac tissue<sup>[60]</sup>. In our study however, despite differences in treatment duration and concentration, both acute high-dose exposure (10  $\mu\text{M}$  for 1 h) and prolonged low-dose exposure (1  $\mu\text{M}$  for 24 h) elicited comparable endothelial responses, including EndMT induction and the secretome that promoted fibroblast activation and senescence, ultimately impairing ECM production. These findings suggest that lowering peak plasma concentrations alone may not be sufficient to prevent the adverse effects of Dox on endothelial- and fibroblast function we observed in our study.

In conclusion, these findings provide novel insights into Dox-induced endothelial dysfunction and the knock-on paracrine effects thereof on dermal fibroblast function. Dox induced EndMT impairs endothelial function and may compromise microvascular function, which is essential for nutrient delivery, oxygenation, and wound healing. Moreover, the exposure to Dox alters the secretome of endothelial cells, which initially promotes fibroblast activation followed by fibroblast senescence and reduced ECM production. These pathological effects of Dox may underlie the impaired connective tissue regeneration and ageing of the skin observed in Dox-treated murine models<sup>[61]</sup> and delayed skin wound healing observed in patients following chemotherapy<sup>[45,62]</sup>. These results underscore the need for therapeutic strategies aimed at preserving vascular health and regulating

endothelial-fibroblast interactions to mitigate ECM disruption and promote effective wound healing in patients undergoing Dox-based chemotherapy.

### **Acknowledgements:**

The authors gratefully acknowledge the contribution of the Residual Tissue Biobank working group, the research team Burn Center, the clinical team, and the patients of the Plastic and Reconstructive Surgery Department, Red Cross Hospital, Beverwijk, The Netherlands, for providing the material used in this study.

### **Funding Statement:**

This work was supported by the China Scholarship Council (Beijing, China, grant number 202008320278 to ZJ) and by the European Union’s Horizon 2020 Marie Skłodowska-Curie Actions – Innovative Training Networks (European Union, grant number 955722 to MLNPG).

### **Author contributions:**

**Zhu Jiang:** Data curation; Formal analysis; Funding acquisition; Investigation; Methodology; Software; Validation; Visualization; Writing - original draft; **Giulia Sorrentino:** Visualization; Formal analysis; Data curation; Writing - review; **Madalena Lopes Natário Pinto Gomes:** Methodology; Writing - review; **Amber Swan-Taylor:** Formal analysis; **Suat Simsek:** Resources; Methodology; Writing - review; **Joris J.T.H. Roelofs:** Supervision; writing – review; **Hans W.M. Niessen:** Resources; Project administration; Conceptualization; Funding acquisition; Methodology; Supervision; Writing – review & editing; **Paul A.J. Krijnen:** Resources; Project administration; Conceptualization; Funding acquisition; Methodology; Supervision; Writing - review & editing;

### **Conflicts of interest:**

On behalf of all authors, the corresponding author states that there is no conflict of interest.

### **Disclosure:**

None

## References

- [1]. Bloom MW, Hamo CE, Cardinale D, Ky B, Nohria A, Baer L, Skopicki H, Lenihan DJ, Gheorghiade M, Lyon AR, et al. Cancer Therapy-Related Cardiac Dysfunction and Heart Failure: Part 1: Definitions, Pathophysiology, Risk Factors, and Imaging. *Circ Heart Fail.* 2016;9:e002661. doi: 10.1161/CIRCHEARTFAILURE.115.002661
- [2]. Bhatia S. Genetics of Anthracycline Cardiomyopathy in Cancer Survivors: JACC: CardioOncology State-of-the-Art Review. *JACC CardioOncol.* 2020;2:539–552. doi: 10.1016/j.jacc.2020.09.006
- [3]. Smith LA, Cornelius VR, Plummer CJ, Levitt G, Verrill M, Canney P, Jones A. Cardiotoxicity of anthracycline agents for the treatment of cancer: systematic review and meta-analysis of randomised controlled trials. *BMC cancer.* 2010;10:1–14.
- [4]. Soultati A, Mountzios G, Avgerinou C, Papaxoinis G, Pectasides D, Dimopoulos MA, Papadimitriou C. Endothelial vascular toxicity from chemotherapeutic agents: preclinical evidence and clinical implications. *Cancer Treat Rev.* 2012;38:473–483. doi: 10.1016/j.ctrv.2011.09.002
- [5]. Diller L, Chow EJ, Gurney JG, Hudson MM, Kadin-Lottick NS, Kawashima TI, Leisenring WM, Meacham LR, Mertens AC, Mulrooney DA, et al. Chronic disease in the Childhood Cancer Survivor Study cohort: a review of published findings. *J Clin Oncol.* 2009;27:2339–2355. doi: 10.1200/JCO.2008.21.1953
- [6]. Lawrence WT, Norton JA, Harvey AK, Gorschboth CM, Talbot TL, Grotendorst GR. Doxorubicin-induced impairment of wound healing in rats. *J Natl Cancer Inst.* 1986;76:119–126.
- [7]. Yilmaz M, Demirdover C, Mola F. Treatment Options in Extravasation Injury: An Experimental Study in Rats. *Plastic and Reconstructive Surgery.* 2002;109:2418–2423.
- [8]. Korać B, Buzadzić B. Doxorubicin toxicity to the skin: possibility of protection with antioxidants enriched yeast. *J Dermatol Sci.* 2001;25:45–52. doi: 10.1016/s0923-1811(00)00106-7
- [9]. Vita JA. Endothelial function. *Circulation.* 2011;124:e906–912. doi: 10.1161/CIRCULATIONAHA.111.078824
- [10]. Kirk T, Ahmed A, Rognoni E. Fibroblast Memory in Development, Homeostasis and Disease. *Cells.* 2021;10. doi: 10.3390/cells10112840
- [11]. Huyan Y, Chen X, Chang Y, Hua X, Fan X, Shan D, Xu Z, Tao M, Zhang H, Liu S, et al. Single-Cell Transcriptomic Analysis Reveals Myocardial Fibrosis Mechanism of Doxorubicin-Induced Cardiotoxicity. *Int Heart J.* 2024;65:487–497. doi: 10.1536/ihj.23-302
- [12]. Espitia-Corredor JA, Shammoun L, Olivares-Silva F, Rimassa-Taré C, Muñoz-Rodríguez C, Espinoza-Pérez C, Sánchez-Ferrer CF, Peiró C, Díaz-Araya G. Resolvin E1 attenuates doxorubicin-induced cardiac fibroblast senescence: A key role for IL-1 $\beta$ . *Biochim Biophys Acta Mol Basis Dis.* 2022;1868:166525. doi: 10.1016/j.bbdis.2022.166525
- [13]. Zeisberg EM, Tarnavski O, Zeisberg M, Dorfman AL, McMullen JR, Gustafsson E, Chandraker A, Yuan X, Pu WT, Roberts AB. Endothelial-to-mesenchymal transition contributes to cardiac fibrosis. *Nature medicine.* 2007;13:952–961.
- [14]. Hashimoto N, Phan SH, Imaizumi K, Matsuo M, Nakashima H, Kawabe T, Shimokata K, Hasegawa Y. Endothelial–mesenchymal transition in bleomycin-induced pulmonary fibrosis. *American journal of respiratory cell and molecular biology.* 2010;43:161–172.
- [15]. Jiang Z, Sorrentino G, Simsek S, Roelofs J, Niessen HWM, Krijnen PAJ. Increased perivascular fibrosis and pro-fibrotic cellular transition in intramyocardial blood vessels in myocardial infarction patients. *J Mol Cell Cardiol Plus.* 2024;10:100275. doi: 10.1016/j.jmccpl.2024.100275
- [16]. Mathivanan S, Ji H, Simpson RJ. Exosomes: extracellular organelles important in intercellular communication. *Journal of proteomics.* 2010;73:1907–1920.
- [17]. Haynes BA, Yang LF, Huyck RW, Lehrer EJ, Turner JM, Barabutis N, Correll VL, Mathiesen A, McPheat W, Semmes OJ, et al. Endothelial-to-Mesenchymal Transition in Human Adipose Tissue Vasculature Alters the Particulate Secretome and Induces Endothelial Dysfunction. *Arteriosclerosis, Thrombosis, and Vascular Biology.* 2019;39:2168–2191. doi: 10.1161/ATVBAHA.119.312826
- [18]. Fyhrquist F, Saijonmaa O, Strandberg T. The roles of senescence and telomere shortening in cardiovascular disease. *Nature Reviews Cardiology.* 2013;10:274–283.
- [19]. Liu D, Liu J, Zhang D, Yang W. Advances in relationship between cell senescence and atherosclerosis. *Zhejiang Da Xue Xue Bao Yi Xue Ban.* 2022;51:95–101. doi: 10.3724/zdxbyxb-2021-0270
- [20]. Han Y, Kim SY. Endothelial senescence in vascular diseases: current understanding and future opportunities in senotherapeutics. *Experimental & Molecular Medicine.* 2023;55:1–12. doi: 10.1038/s12276-022-00906-w

- [21]. Lipphardt M, Song JW, Matsumoto K, Dadafarin S, Dihazi H, Müller G, Goligorsky MS. The third path of tubulointerstitial fibrosis: aberrant endothelial secretome. *Kidney International*. 2017;92:558–568. doi: <https://doi.org/10.1016/j.kint.2017.02.033>
- [22]. van den Bogaardt AJ, van Zuijlen PP, van Galen M, Lamme EN, Middelkoop E. The suitability of cells from different tissues for use in tissue-engineered skin substitutes. *Arch Dermatol Res*. 2002;294:135–142. doi: 10.1007/s00403-002-0305-3
- [23]. Mross K, Maessen P, van der Vijgh WJ, Gall H, Boven E, Pinedo HM. Pharmacokinetics and metabolism of epidoxorubicin and doxorubicin in humans. *J Clin Oncol*. 1988;6:517–526. doi: 10.1200/JCO.1988.6.3.517
- [24]. Chomczynski P, Sacchi N. Single-step method of RNA isolation by acid guanidinium thiocyanate-phenol-chloroform extraction. *Analytical Biochemistry*. 1987;162:156–159. doi: [https://doi.org/10.1016/0003-2697\(87\)90021-2](https://doi.org/10.1016/0003-2697(87)90021-2)
- [25]. Lee KN, Jackson KW, Christiansen VJ, Chung KH, McKee PA. A novel plasma proteinase potentiates  $\alpha$ 2-antiplasmin inhibition of fibrin digestion. *Blood*. 2004;103:3783–3788. doi: <https://doi.org/10.1182/blood-2003-12-4240>
- [26]. Hernandez-Segura A, Nehme J, Demaria M. Hallmarks of Cellular Senescence. *Trends in Cell Biology*. 2018;28:436–453. doi: <https://doi.org/10.1016/j.tcb.2018.02.001>
- [27]. Quan T, Xia W, He T, Calderone K, Bou-Gharios G, Voorhees JJ, Dlugosz AA, Fisher GJ. Matrix Metalloproteinase-1 Expression in Fibroblasts Accelerates Dermal Aging and Promotes Papilloma Development in Mouse Skin. *Journal of Investigative Dermatology*. 2023;143:1700–1707.e1701. doi: <https://doi.org/10.1016/j.jid.2023.02.028>
- [28]. Cho JG, Lee A, Chang W, Lee MS, Kim J. Endothelial to Mesenchymal Transition Represents a Key Link in the Interaction between Inflammation and Endothelial Dysfunction. *Front Immunol*. 2018;9:294. doi: 10.3389/fimmu.2018.00294
- [29]. Sun X, Nkenor B, Mastikhina O, Soon K, Nunes SS. Endothelium-mediated contributions to fibrosis. *Seminars in Cell & Developmental Biology*. 2020;101:78–86. doi: <https://doi.org/10.1016/j.semcdb.2019.10.015>
- [30]. Yin Z, Zhao Y, Li H, Yan M, Zhou L, Chen C, Wang DW. miR-320a mediates doxorubicin-induced cardiotoxicity by targeting VEGF signal pathway. *Aging (Albany NY)*. 2016;8:192.
- [31]. Tsai TH, Lin CJ, Hang CL, Chen WY. Calcitriol Attenuates Doxorubicin-Induced Cardiac Dysfunction and Inhibits Endothelial-to-Mesenchymal Transition in Mice. *Cells*. 2019;8. doi: 10.3390/cells8080865
- [32]. Wang-Evers M, Casper MJ, Glahn J, Luo T, Doyle AE, Karasik D, Kim AC, Phothong W, Nathan NR, Heesakker T, et al. Assessing the impact of aging and blood pressure on dermal microvasculature by reactive hyperemia optical coherence tomography angiography. *Scientific Reports*. 2021;11:13411. doi: 10.1038/s41598-021-92712-z
- [33]. Zeng H, Chen JX. Microvascular Rarefaction and Heart Failure With Preserved Ejection Fraction. *Front Cardiovasc Med*. 2019;6:15. doi: 10.3389/fcvm.2019.00015
- [34]. Lu Y, Yang Y, Xiao L, Li S, Liao X, Liu H. Autocrine and Paracrine Effects of Vascular Endothelial Cells Promote Cutaneous Wound Healing. *Biomed Res Int*. 2021;2021:6695663. doi: 10.1155/2021/6695663
- [35]. Tan Y, Zhang M, Kong Y, Zhang F, Wang Y, Huang Y, Song W, Li Z, Hou L, Liang L, et al. Fibroblasts and endothelial cells interplay drives hypertrophic scar formation: Insights from in vitro and in vivo models. *Bioeng Transl Med*. 2024;9:e10630. doi: 10.1002/btm2.10630
- [36]. Widyantoro B, Emoto N, Nakayama K, Anggrahini DW, Adiarto S, Iwasa N, Yagi K, Miyagawa K, Rikitake Y, Suzuki T. Endothelial cell-derived endothelin-1 promotes cardiac fibrosis in diabetic hearts through stimulation of endothelial-to-mesenchymal transition. *Circulation*. 2010;121:2407–2418.
- [37]. Sinitskaya AV, Velikanova EA, Senokosova EA, Sinitsky MY, Khutornaya MV, Asanov MA, Poddubnyak AO, Ponasenkov AV. The cytokine response of human coronary artery endothelial cells treated with doxorubicin: results of an in vitro experiment. *Biomed Khim*. 2024;70:156–160. doi: 10.18097/pbmc20247003156
- [38]. Takagaki Y, Lee SM, Dongqing Z, Kitada M, Kanasaki K, Koya D. Endothelial autophagy deficiency induces IL6 - dependent endothelial mesenchymal transition and organ fibrosis. *Autophagy*. 2020;16:1905–1914. doi: 10.1080/15548627.2020.1713641
- [39]. Johnson BZ, Stevenson AW, Prête CM, Fear MW, Wood FM. The Role of IL-6 in Skin Fibrosis and Cutaneous Wound Healing. *Biomedicine*. 2020;8. doi: 10.3390/biomedicine8050101
- [40]. Li Y, Zhao J, Yin Y, Li K, Zhang C, Zheng Y. The Role of IL-6 in Fibrotic Diseases: Molecular and Cellular

- Mechanisms. *Int J Biol Sci.* 2022;18:5405–5414. doi: 10.7150/ijbs.75876
- [41]. Cao C, Xu W, Lei J, Zheng Y, Zhang A, Xu A, Lin F, Zhou M. The IL-6 autocrine loop promoting IFN- $\gamma$ -induced fibroblast senescence is involved in psychological stress-mediated exacerbation of vitiligo. *Inflammation Research.* 2025;74:72. doi: 10.1007/s00011-025-02035-2
- [42]. Liu Z, Jiang Y, Li Y, Wang J, Fan L, Scott MJ, Xiao G, Li S, Billiar TR, Wilson MA, et al. TLR4 Signaling Augments Monocyte Chemotaxis by Regulating G Protein–Coupled Receptor Kinase 2 Translocation. *The Journal of Immunology.* 2013;191:857–864. doi: 10.4049/jimmunol.1300790
- [43]. Deshmane SL, Kremlev S, Amini S, Sawaya BE. Monocyte chemoattractant protein-1 (MCP-1): an overview. *J Interferon Cytokine Res.* 2009;29:313–326. doi: 10.1089/jir.2008.0027
- [44]. Roubenoff R, Harris TB, Abad LW, Wilson PW, Dallal GE, Dinarello CA. Monocyte cytokine production in an elderly population: effect of age and inflammation. *J Gerontol A Biol Sci Med Sci.* 1998;53:M20–26. doi: 10.1093/gerona/53a.1.m20
- [45]. Stonimska P, Sachadyn P, Zieliński J, Skrzypski M, Piłkuta M. Chemotherapy-Mediated Complications of Wound Healing: An Understudied Side Effect. *Adv Wound Care (New Rochelle).* 2024;13:187–199. doi: 10.1089/wound.2023.0097
- [46]. Rinkevich Y, Walmsley GG, Hu MS, Maan ZN, Newman AM, Drukker M, Januszzyk M, Krampitz GW, Gurtner GC, Lorenz HP, et al. Skin fibrosis. Identification and isolation of a dermal lineage with intrinsic fibrogenic potential. *Science.* 2015;348:aaa2151. doi: 10.1126/science.aaa2151
- [47]. Darby IA, Laverdet B, Bonté F, Desmoulière A. Fibroblasts and myofibroblasts in wound healing. *Clin Cosmet Investig Dermatol.* 2014;7:301–311. doi: 10.2147/ccid.S50046
- [48]. Podyacheva E, Shmakova T, Kushnareva E, Onopchenko A, Martynov M, Andreeva D, Toropov R, Cheburkin Y, Levchuk K, Goldaeva A, et al. Modeling Doxorubicin-Induced Cardiomyopathy With Fibrotic Myocardial Damage in Wistar Rats. *Cardiol Res.* 2022;13:339–356. doi: 10.14740/cr1416
- [49]. Levick SP, Soto-Pantoja DR, Bi J, Hundley WG, Widiapradja A, Manteufel EJ, Bradshaw TW, Meléndez GC. Doxorubicin-Induced Myocardial Fibrosis Involves the Neurokinin-1 Receptor and Direct Effects on Cardiac Fibroblasts. *Heart Lung Circ.* 2019;28:1598–1605. doi: 10.1016/j.hlc.2018.08.003
- [50]. Patricelli C, Lehmann P, Oxford JT, Pu X. Doxorubicin-induced modulation of TGF- $\beta$  signaling cascade in mouse fibroblasts: insights into cardiotoxicity mechanisms. *Scientific Reports.* 2023;13:18944. doi: 10.1038/s41598-023-46216-7
- [51]. Pullar JM, Carr AC, Vissers MCM. The Roles of Vitamin C in Skin Health. *Nutrients.* 2017;9. doi: 10.3390/nu9080866
- [52]. Pitiyage GN, Slijepcevic P, Gabrani A, Chianea YG, Lim KP, Prime SS, Tilakaratne WM, Fortune F, Parkinson EK. Senescent mesenchymal cells accumulate in human fibrosis by a telomere-independent mechanism and ameliorate fibrosis through matrix metalloproteinases. *J Pathol.* 2011;223:604–617. doi: 10.1002/path.2839
- [53]. Gerasymchuk M, Robinson GI, Kovalchuk O, Kovalchuk I. Modeling of the Senescence-Associated Phenotype in Human Skin Fibroblasts. *Int J Mol Sci.* 2022;23. doi: 10.3390/ijms23137124
- [54]. Fisher GJ, Wang B, Cui Y, Shi M, Zhao Y, Quan T, Voorhees JJ. Skin aging from the perspective of dermal fibroblasts: the interplay between the adaptation to the extracellular matrix microenvironment and cell autonomous processes. *J Cell Commun Signal.* 2023;17:523–529. doi: 10.1007/s12079-023-00743-0
- [55]. Varani J, Dame MK, Rittie L, Fligiel SE, Kang S, Fisher GJ, Voorhees JJ. Decreased collagen production in chronologically aged skin: roles of age-dependent alteration in fibroblast function and defective mechanical stimulation. *Am J Pathol.* 2006;168:1861–1868. doi: 10.2353/ajpath.2006.051302
- [56]. Ardi VC, Van den Steen PE, Opdenakker G, Schweighofer B, Deryugina EI, Quigley JP. Neutrophil MMP-9 Proenzyme, Unencumbered by TIMP-1, Undergoes Efficient Activation in Vivo and Catalytically Induces Angiogenesis via a Basic Fibroblast Growth Factor (FGF-2)/FGFR-2 Pathway\*. *Journal of Biological Chemistry.* 2009;284:25854–25866. doi: <https://doi.org/10.1074/jbc.M109.033472>
- [57]. Wang X, Khalil RA. Matrix Metalloproteinases, Vascular Remodeling, and Vascular Disease. *Adv Pharmacol.* 2018;81:241–330. doi: 10.1016/bs.apha.2017.08.002
- [58]. Caley MP, Martins VL, O'Toole EA. Metalloproteinases and Wound Healing. *Adv Wound Care (New Rochelle).* 2015;4:225–234. doi: 10.1089/wound.2014.0581
- [59]. Visse R, Nagase H. Matrix metalloproteinases and tissue inhibitors of metalloproteinases: structure, function, and biochemistry. *Circ Res.* 2003;92:827–839. doi: 10.1161/01.Res.0000070112.80711.3d
- [60]. Legha SS, Benjamin RS, Mackay B, Ewer M, Wallace S, Valdivieso M, Rasmussen SL, Blumenschein

- GR, Freireich EJ. Reduction of doxorubicin cardiotoxicity by prolonged continuous intravenous infusion. *Ann Intern Med.* 1982;96:133–139. doi: 10.7326/0003-4819-96-2-133
- [61]. Demaria M, O'Leary MN, Chang J, Shao L, Liu S, Alimirah F, Koenig K, Le C, Mitin N, Deal AM, et al. Cellular Senescence Promotes Adverse Effects of Chemotherapy and Cancer Relapse. *Cancer Discov.* 2017;7:165–176. doi: 10.1158/2159-8290.Cd-16-0241
- [62]. Deptuła M, Zieliński J, Wardowska A, Pikuta M. Wound healing complications in oncological patients: perspectives for cellular therapy. *Postepy Dermatol Alergol.* 2019;36:139–146. doi: 10.5114/ada.2018.72585

**Table S1. Chemicals and reagents used in this study**

<b>Name</b>	<b>Source</b>	<b>Code number or CAS number</b>
Endothelial Cell Medium (ECM)	ScienCell (USA)	#1001
Dulbecco's Modified Eagle Medium (DMEM)	Thermo Scientific (USA)	41966029
Endothelial cell growth supplement	ScienCell (USA)	#1052
Penicillin/streptomycin solution	ScienCell (USA)	#0503
	Thermo Scientific (USA)	15140-122
Fetal bovine serum (FBS)	ScienCell (USA)	#0025
	Sigma-Aldrich (USA)	F7524
GlutaMAX	Thermo Scientific (USA)	35050-038
Prolong Gold antifade reagent	Thermo Scientific (USA)	P36934
Doxorubicin hydrochloride	Sigma-Aldrich (St. Louis, MO, USA)	25316-40-9 (D1515-10mg)
Dimethylsulfoxide (DMSO)	Sigma-Aldrich (St. Louis, MO, USA)	67-68-5
$\beta$ -mercaptoethanol	Sigma-Aldrich (St. Louis, MO, USA)	M3148
SDS	Bio-Rad Laboratories (USA)	#1610418
Tris	Thermo Scientific (USA)	15504-020
Tween 20	Sigma-Aldrich (St. Louis, MO, USA)	P1379
Bovine Serum Albumin Fraction V (BSA)	Sigma-Aldrich (St. Louis, MO, USA)	10735094001
Sodium azide ( $\text{NaN}_3$ )	Sigma-Aldrich (St. Louis, MO, USA)	K38256488 843
TRI Reagent (Trizol)	Sigma-Aldrich (St. Louis, MO, USA)	T9424
Bromophenol blue	Sigma-Aldrich (St. Louis, MO, USA)	MFCD00005875